Establishing A Mapping Methodology For NSCAT Winds

by S. Dickinson, S. Singh, K.A. Kelly, M. Spillane, and M.J. McPhaden

Technical Report
APL-UW TR 9801
April 1998

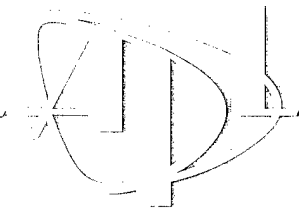

Applied Physics Laboratory University of Washington
Seattle, Washington 98105-6698

JPL/NASA NSCAT Science Working Team #960927
UW(JISAO) - NOAA Cooperative Agreement # NA67RJ0155

Establishing A Mapping Methodology For NSCAT Winds

by S. Dickinson, S. Singh, K.A. Kelly, M. Spillane,
and M.J. McPhaden

Technical Report
APL-UW TR 9801
April 1998

Applied Physics Laboratory **University of Washington**
1013 NE 40th Street Seattle, Washington 98105-6698

JPL/NASA NSCAT Science Working Team #960927
UW(JISAO) - NOAA Cooperative Agreement # NA67RJ0155

ACKNOWLEDGMENTS

We would like to thank the following sponsors for their support of this work: NSCAT Science Working Team, NOAA's National Environmental Satellite, Data, and Information Service (NESDIS), NOAA's Office of Global Programs (OGP), and NOAA's Office of Oceanic and Atmospheric Research (OAR).

We also acknowledge Pat Phoebus at the Fleet Numerical Meteorology and Oceanography Center, Naval Research Laboratory, for the T79 NOGAPS model output; Michael Freilich at Oregon State University, for the orbit program and NSCAT sampling pattern; the European Centre for Medium-range Weather Forecasts, for analysis winds; the NSCAT Project Office and the Physical Oceanography Distributed Active Archive Center at the Jet Propulsion Laboratory, for scatterometer data; and the Center for Ocean Atmosphere Prediction Studies, Florida State University, for climatological monthly means of pseudostress.

This work was sponsored under NASA contract 960927 and UW-NOAA cooperative agreement NA67RJ0155.

ABSTRACT

A methodology is presented for mapping swath-oriented NASA scatterometer (NSCAT) wind data into gridded maps suitable for forcing ocean circulation models. NSCAT samples the winds over the equatorial Pacific Ocean unevenly in both space and time, and care must be taken in mapping them onto a grid to prevent aliasing the fields. It was necessary to develop a "true" wind field with which to test the mapping methodology. Prior to the availability of NSCAT data, the European Centre for Medium-Range Weather Forecasts (ECMWF) and Fleet Numerical Meteorology and Oceanography Center (FNMOC) analysis wind fields were studied. Spectral analysis of the ECMWF and FNMOC wind fields showed a drastic drop in energy at scales smaller than 600 km. These energy levels were "pumped up" in the Fourier domain to represent a true wind field more accurately. These "true" wind fields were converted to pseudostress, subsampled with the known NSCAT sampling pattern (termed "synthetic NSCAT" winds), and then objectively averaged. A study of the expected errors of the mapped pseudostress was conducted using a covariance function of the equatorial Pacific wind field determined with data from the Tropical Atmosphere Ocean (TAO) buoy array. A 5-day, 2° resolution was chosen for the daily mapped pseudostress. Comparisons of the "true" winds converted to pseudostress and the mapped synthetic NSCAT pseudostress show errors consistent with the expected values. Maps made of actual NSCAT data are also presented and discussed.

TABLE OF CONTENTS

LIST OF FIGURES

I. INTRODUCTION

For many uses of the wind measurements from the NASA scatterometer (NSCAT), it is necessary to convert the swath-oriented data to a uniform grid spatially and temporally. This can be done either by assimilation into an atmospheric general circulation model (AGCM) or by interpolation of the actual data. We have chosen the latter method, in the expectation that there are oceanographically important structures in the wind field with spatial resolution finer than can be obtained using an AGCM and that there are oceanographic processes that do not suffer from the decrease in temporal resolution necessary to produce such a data product. We selected the appropriate mapping parameters and tested the accuracy of the mapping procedure by using realistic simulated wind fields. In addition, we present results using actual NSCAT data.

This report details the mapping methodology. In particular, it discusses

- development of a data set (representing the true wind fields) used to establish map parameters
- determination of the covariance function for the Pacific Ocean equatorial winds
- the mapping algorithm, including the objective averaging technique
- analysis of estimated mapping errors and actual errors.

Two sets of analysis wind fields were used in developing the mapping algorithm. The first was 12-hourly vectors (0000Z and 1200Z) for March 1993 from the Navy's T79 NOGAPS model, obtained from P. Phoebus at the Fleet Numerical Meteorology and Oceanography Center (FNMOC) in Monterey, California. This period had a westerly wind burst early in the month (starting 6 March), which later developed into a twin cyclone (see Figure 1). There was a weaker westerly episode around 20 March. The output of the T79 model was gridded to 1° in both latitude and longitude; however, it is a spectral model and has an effective resolution of only about 1.5°. The second analysis wind product was 6-hourly 10-m wind vectors for January 1991 through March 1993 from the European Centre for Medium-range Weather Forecasts (ECMWF) at a spatial grid of approximately 1.125° by 1.125°.

Both products are too smooth to determine whether maps constructed from scatterometer data will resolve the smaller spatial scales expected in the actual wind field. Therefore, it was necessary to add those smaller spatial scales by altering the data in the spectral domain, as done by Kelly and Caruso (1990). These spectrally modified wind vectors were then considered the "true" winds for testing the map methodology and were subsampled using the known measurement pattern of NSCAT ("synthetic NSCAT" data). Daily wind maps were reconstructed from these subsampled vectors and were compared with the "true" winds to determine the accuracy of the maps.

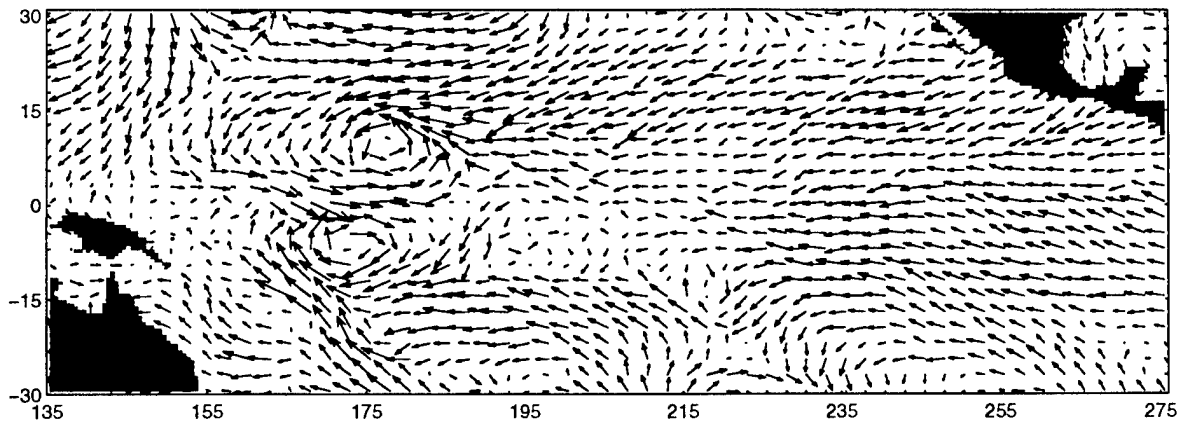

Figure 1. Example of NOGAPS wind field from FNMOC showing the westerly wind burst associated with a pair of cyclones.

II. CONSTRUCTION OF DATA SETS

A. "True" Winds

Spatial spectra estimated by Freilich and Chelton (1986) from the Seasat-A Satellite Scatterometer (SASS) for the tropical Pacific Ocean suggest that the spectral shape of vector wind fields should be approximately $k^{-1.8}$. Both the FNMOC and the ECMWF wind fields for this region were interpolated to a $0.5° \times 0.5°$ grid, extending the Nyquist wavenumber of the fields to correspond to smaller spatial scales. Average spectra for these regridded fields were computed and compared with the $k^{-1.8}$ line. The ratio between the $k^{-1.8}$ spectra and average spectra from 2 years of original ECMWF wind fields (January 1993 through December 1994) was computed. The square root of this ratio is used to calculate the factors with which to "pump up" the wind Fourier magnitudes. For very low wavenumbers ($< 10^{-3}$), the factor is set to 1. For higher wavenumbers (between 10^{-3} and 10^{-2}), the factor is first converted to a function of radial wavenumber and then boxcar filtered to smooth spikes. This radial factor is then splined onto the entire Fourier field, obtaining a smooth field of factors. The Fourier magnitudes from each component field were then individually multiplied by the factors, so that, on average, the modified wind fields had spectra of approximately $k^{-1.8}$ (Figures 2 and 3). The phase for each component was unchanged. One set of factors was used on all the wind maps for the entire data record. Only those Fourier magnitudes corresponding to spatial scales between about 600 and 100 km (the original Nyquist wavenumber) were modified. Increasing the spectra for smaller wavenumbers results in "ringing" when the fields are inversely transformed and does not appreciably increase the variance in the fields. Although the modified spectra for $k<10^{-3}$ should not have been affected, some energy leaked from the higher frequencies (lower wavenumbers). Note that the FNMOC winds had considerably less energy at the smaller spatial scales than the ECMWF winds, and thus it was necessary to make a larger alteration to the Fourier magnitudes, which resulted in some ringing in the modified FNMOC fields. Although the ECMWF 10-m analysis winds also lack energy at the higher frequencies, as can be seen in Figure 3, the ECMWF wind fields were used in the final testing because the ECMWF spectral modification was more accurate.

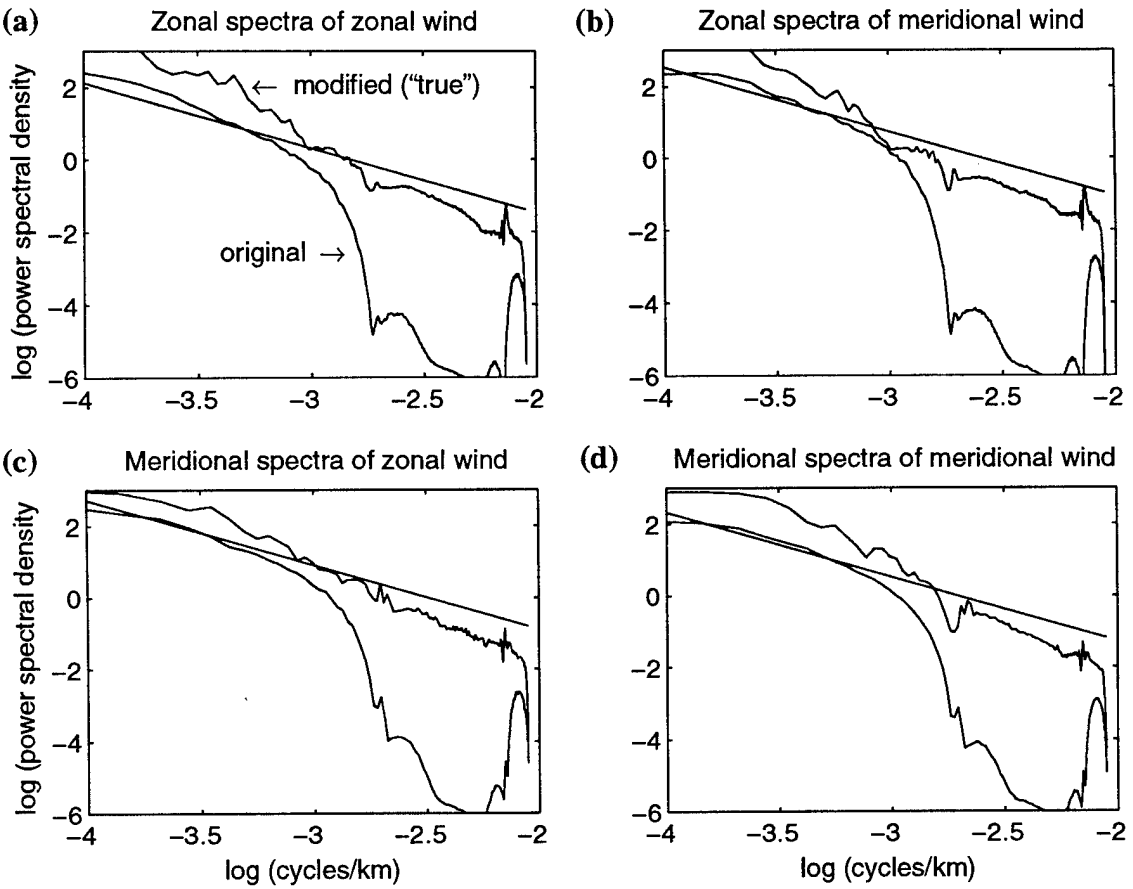

Figure 2. Wavenumber spectra for original FNMOC wind fields and spectrally modified, or "true," fields. (a) Zonal spectra of zonal wind, (b) zonal spectra of meridional wind, (c) meridional spectra of zonal wind, and (d) meridional spectral of meridional wind. The $k^{-1.8}$ spectrum (shown as a straight line in all plots) was used as a guide to modify the wind components. The spectra of the modified ("true") data fall nearly along this line.

To quantify the changes in the FNMOC wind field due to altering the spectrum, the spatially averaged variances and temporal decorrelation (e-folding) times were computed for each component for both the original FNMOC winds and the spectrally modified FNMOC winds (Table 1). The values of the variance (relative to the mean for the month of March 1993) of the zonal and meridional components increased by about 9% and 4%, respectively; the temporal decorrelation times decreased by about 12% and 14%, respectively.

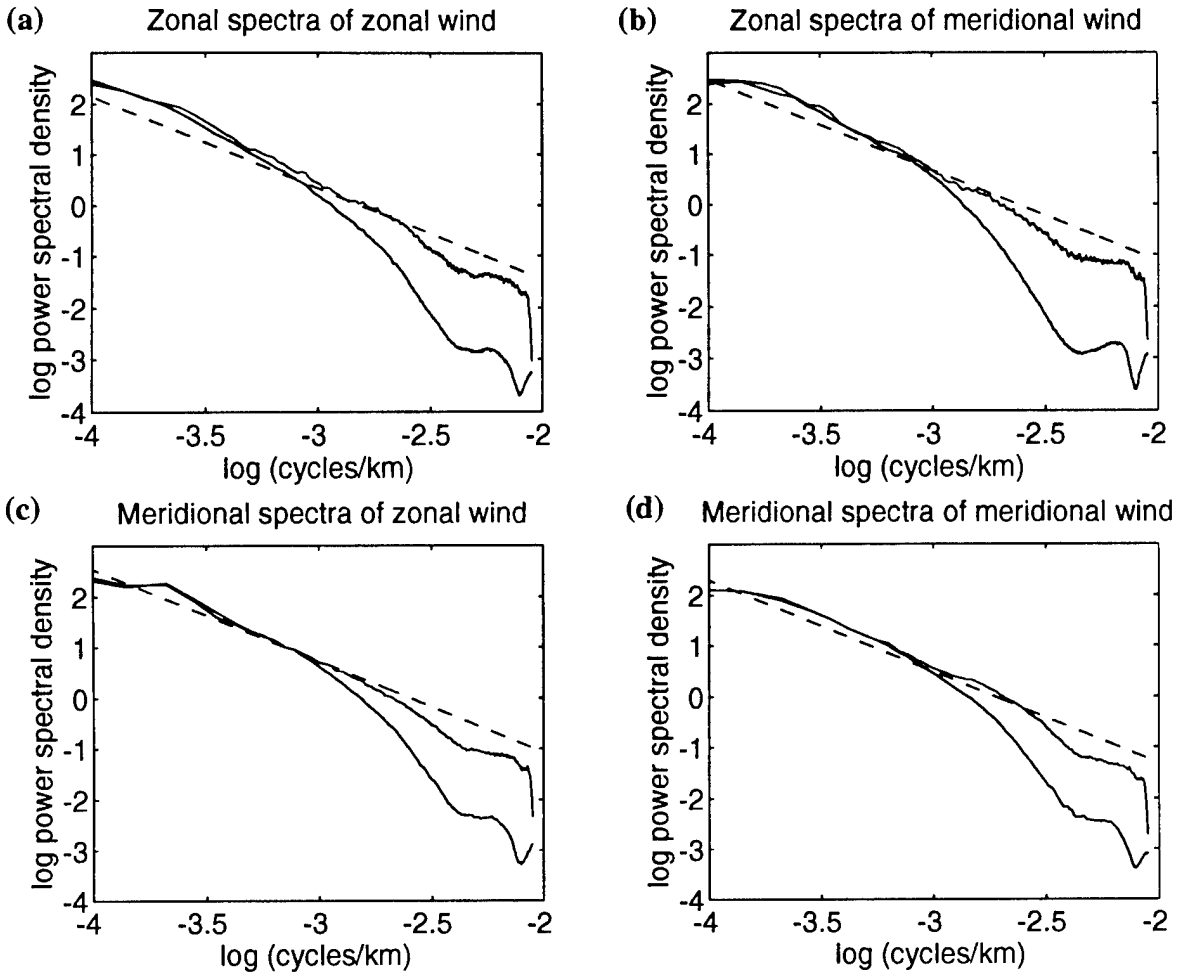

Figure 3. Same as Figure 2, except for ECMWF wind fields. The original ECMWF winds had significantly more energy than the FNMOC winds at scales shorter than 1000 km (10^{-3} cycles/km), which made the spectral modification more accurate. (Note: This is why final testing was done using ECMWF wind fields.)

Table 1. Comparison of spatially averaged variances and temporal decorrelation for FNMOC and spectrally modified FNMOC winds.

Parameter	FNMOC	Spectrally Modified FNMOC
Zonal Variance (m^2/s^2)	6.4	7.0
Meridional Variance (m^2/s^2)	4.8	5.0
Time Scale, Zonal Component (hr)	47	41
Time Scale, Meridional Component (hr)	29	25

Finally, the pumping factors are applied to sample fields to check the procedure. Figure 4 shows the original and "true" zonal component of the wind on 1 January 1993. Figure 5 shows the difference in the vector field. The differences are confined mostly to the high-wavenumber features, sharpening fronts. Some small, unrealistic features are also added.

B. Synthetic NSCAT Data

ECMWF winds from September 1992 through March 1993 were spectrally modified to produce a set of "true" winds. These "true" winds were then subsampled, using the known instrument sampling pattern and the expected orbit for the ADEOS-I (ADvanced Earth Observing System) satellite [courtesy of M. Freilich] for the entire record. As an approximation to the actual sampling, we selected the "true" wind vector closest spatially (within 0.5°) and temporally (within 6 hours) to each actual sample location and time. To illustrate the density of wind vector measurements from NSCAT, the number of wind vectors available for 12-hour, 24-hour, and 48-hour time periods are shown in Figure 6. In the top panel the double-swath pattern of the instrument is readily apparent, with the relatively narrow nadir gap (350 km with no data) between the parallel swaths. The swaths from five

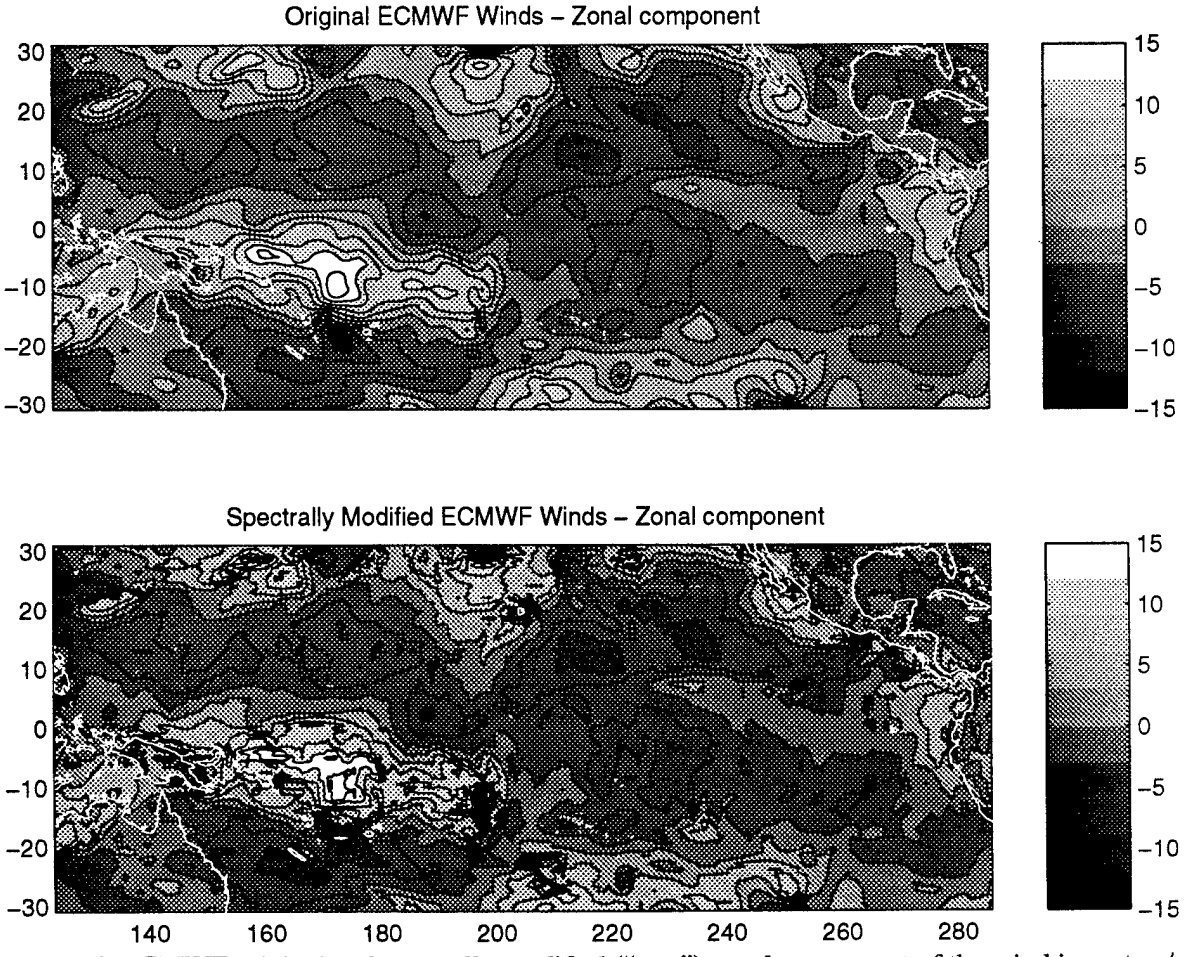

Figure 4. ECMWF original and spectrally modified ("true") zonal component of the wind in meters/second, 1 January 1993.

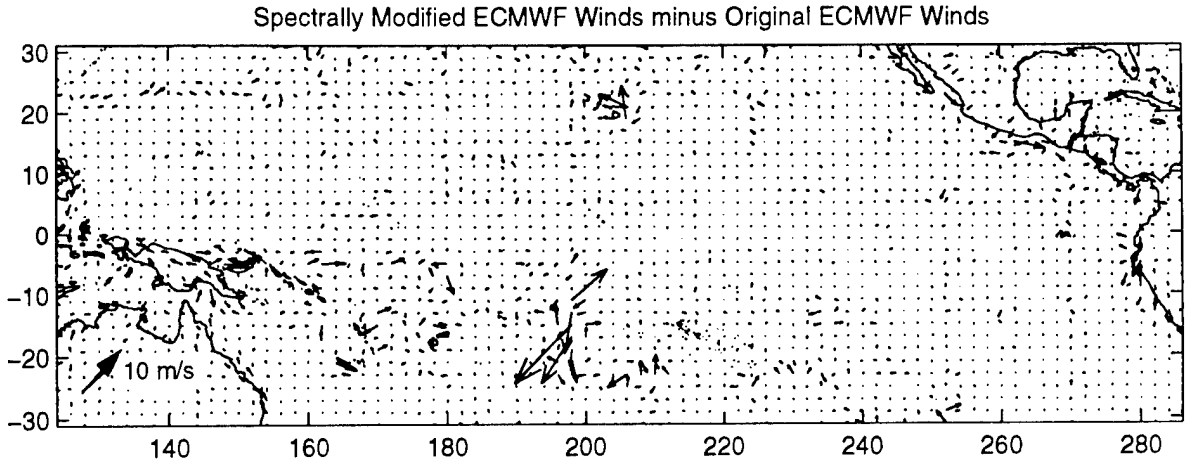

Figure 5. Difference between original and spectrally modified ECMWF 10-m winds shown in Figure 4. Spectrally modified winds contain more energy at the smaller spatial scales by design.

complete successive descending (northeast-to-southwest tending) subtracks and one ascending subtrack (left side of the figure) are shown. Note also the absence of wind measurements over land. In a 24-hour period, most of the previous gaps have been crossed by subsequent swaths, but there are still relatively large regions without data. By the end of the 48-hour period, the largest gaps are less than 5° in longitude and 10° in latitude.

The subsampled "true" winds (synthetic NSCAT winds) are then used to create daily maps on a $1° \times 1°$ grid, simulating the process used to make maps from actual NSCAT data. The quantity ultimately needed to drive an ocean model is the wind stress, and because of the nonlinear relationship between vector winds and stress, we first converted the subsampled winds to "pseudostress" and then applied our mapping algorithms as will be discussed in Section 4. (Pseudostress is simply the stress divided by the drag coefficient and air density.)

To make maps from these data sets (synthetic as well as actual NSCAT data), some statistics of the Pacific equatorial wind field are needed. The mapping algorithm includes a so-called "objective estimate" of the temporal mean stress, so it is necessary to estimate the time-lagged autocovariance of the stress components, which is the subject of Section 3.

To check the accuracy of the mapping algorithm, the synthetic NSCAT stress fields were mapped and compared with the "true" stress fields. The availability of both the mapped and the "true" stress fields allowed two types of comparisons to be made: first, statistical comparisons of the estimated and actual errors of the NSCAT sampling/mapping procedure and, second, forcing of a tropical ocean circulation model with both stress fields to determine its sensitivity to expected errors in the NSCAT stress maps. Only the first set of comparisons is discussed in this report, in Section 5.

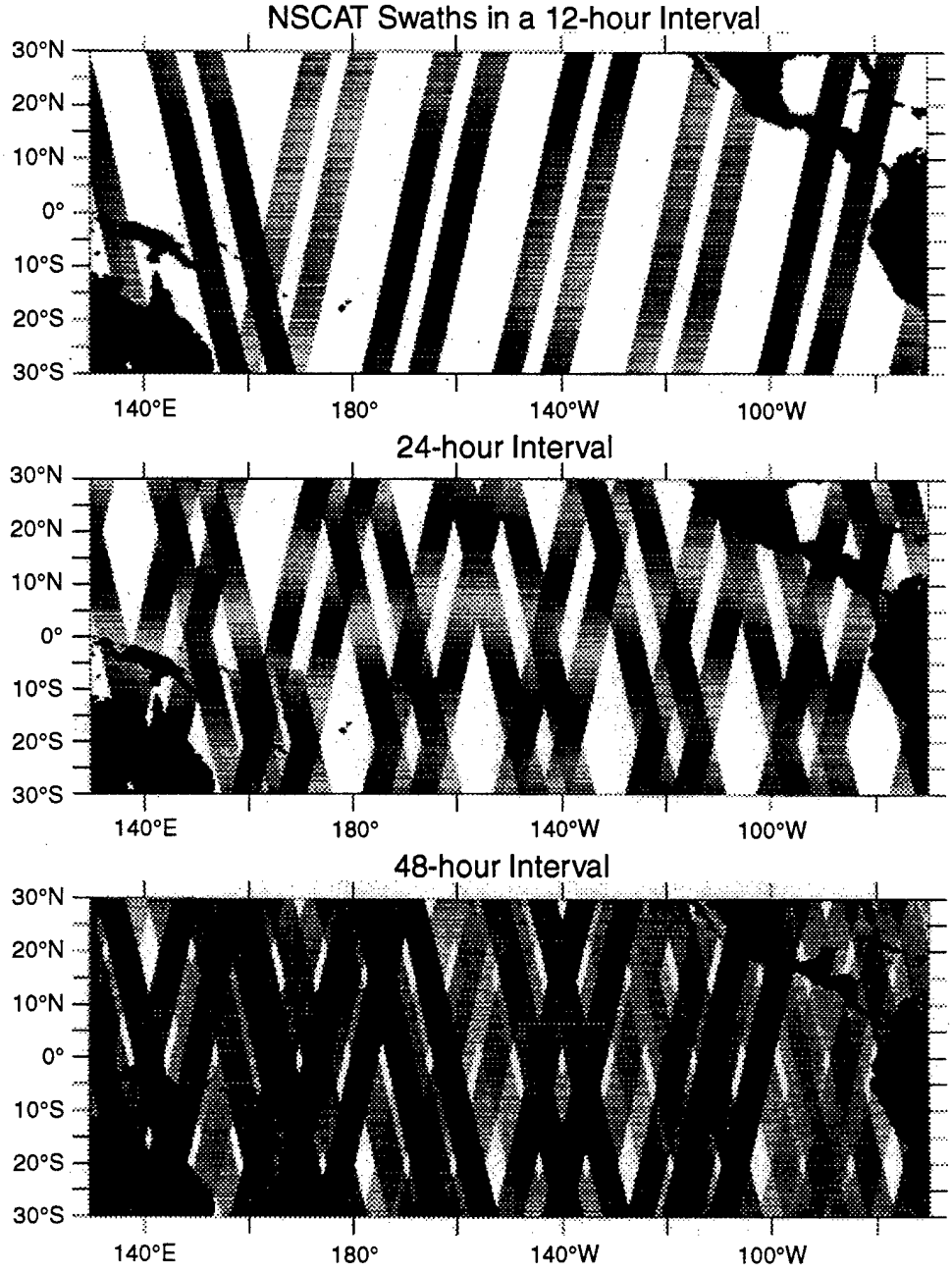

Figure 6. Sampling pattern of the NASA scatterometer, showing the coverage in 12 hours, 24 hours, and 48 hours. After 2 days there are areas that the satellite does not sample and areas that the satellite passes over several times.

III. COVARIANCE FUNCTIONS FOR EQUATORIAL WINDS

Two years of hourly wind data from 34 of the 77 moored TAO buoys (McPhaden, 1995) were used to determine the covariance function of the Pacific equatorial winds. The locations of the 34 buoys are shown in Figure 7. The "hourly winds" are 6-minute averages centered at the top of each hour from 15 March 1993 through 16 March 1995. The pseudostress components were calculated from the wind data. The time mean was then removed from the time series at each buoy, and the autocorrelation functions were computed.

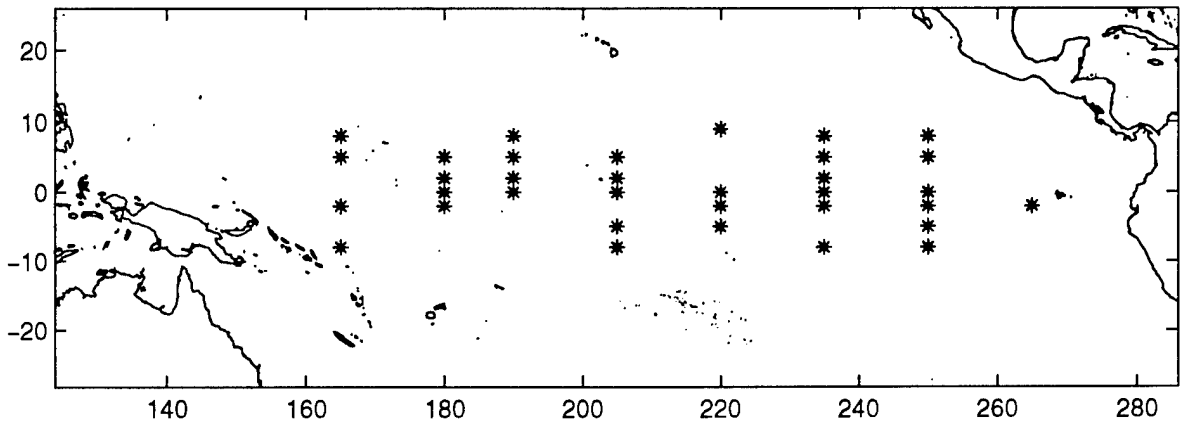

Figure 7. Locations of 34 TAO buoys used to determine the correlation functions for the zonal and meridional winds. Two years of hourly data from each location are used.

Complete time series facilitate computation of the autocovariances; therefore, missing data were replaced by using one of three methods, depending on the length of the gap. Minor gaps (less than 12 hours) in the TAO buoy wind data sets were filled by linear interpolation of daily averages. Somewhat larger gaps (up to 5 days) were filled by autoregression on the neighboring location(s). Longer gaps were filled by regression on 12 hourly ECMWF winds and then linearly interpolated.

Seasonal signals cause the autocorrelation function to remain high at large temporal lags. To get a better estimate of the anomaly decorrelation time scale, the Florida State University (FSU) climatological values for pseudostress were subtracted prior to calculating the autocorrelation function. For this purpose the FSU climatology at the 34 locations was expressed in terms of the first four harmonics of the annual signal. We refer to the autocorrelation functions computed with only the record mean removed from the series as the *raw* cases and autocorrelation functions computed with the FSU climatology removed from the series as the *anomaly* cases.

The autocorrelations with lags out to 120 hours were computed for the raw and anomaly series of both components of the pseudostress. Average autocorrelation functions for raw and

anomaly zonal and meridional pseudostress components are plotted in Figure 8. To simplify the calculation of an objective estimate, an analytic form of the autocorrelation function is needed. An exponential curve fit of the form

$$\hat{c}(\Delta t) = \exp(-|\Delta t|/B) \tag{1}$$

was used over a range of times (Δt) between 0 and 48 hours. Although the use of a double exponential curve fit was also examined, it did not produce an appreciably better fit. The range for the best fit was shifted to 12–60 hours, a range which should include at least four measurements (see Figure 6); this resulted in a better fit to the steeper part of the autocorrelation function (Figure 8) and an underestimate of correlations at longer lags. In the mapping procedure used (Section 4), the autocorrelation function is integrated temporally to produce an objective estimate of the temporally averaged fields and is therefore less sensitive to details of the autocorrelation function than in the usual objective estimate. The zonal pseudostress anomaly decorrelation time, B in Eq. (1), is 49 hours for zonal pseudostress and 29 hours for meridional pseudostress.

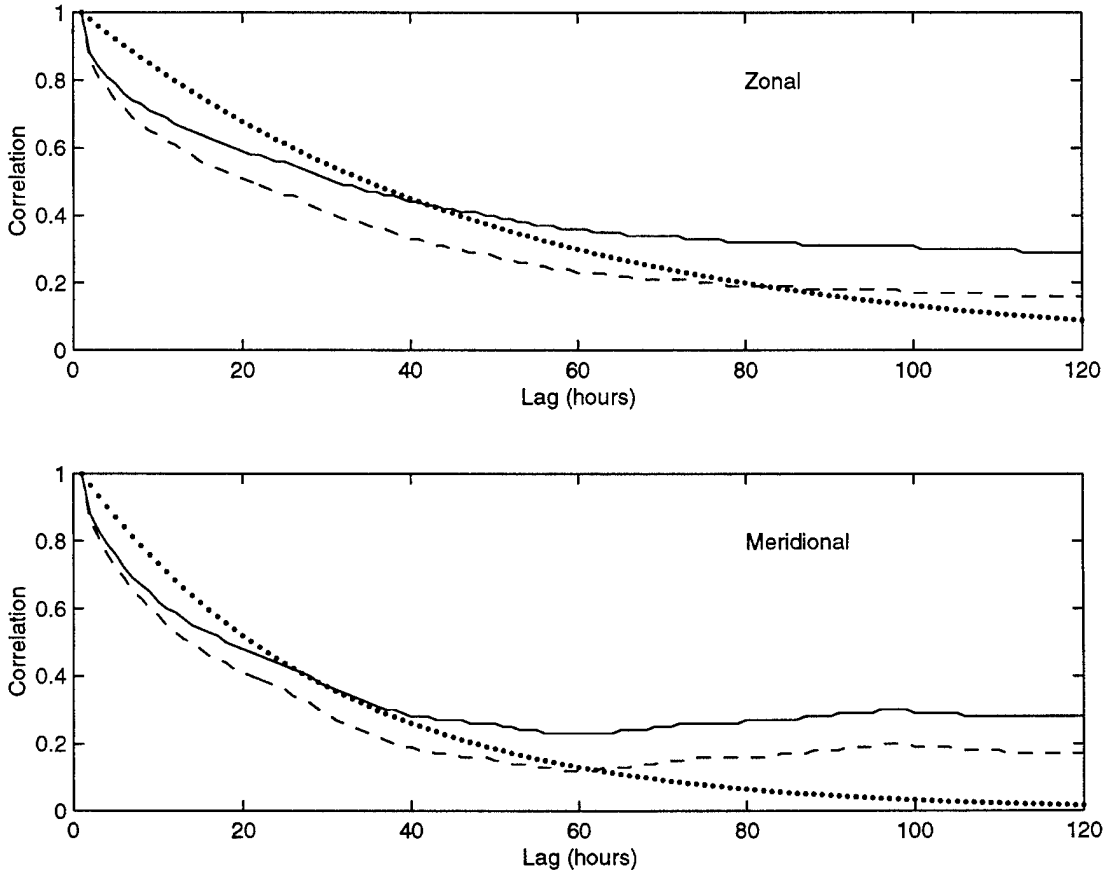

Figure 8: The average autocorrelation function for the pseudostress from the data at the 34 TAO buoys. Autocorrelation functions from the raw pseudostress are solid, and from the anomaly pseudostress are dashed. The dots represent the curve fit, Eq. (1), with B equal to 49 and 29 for the zonal and meridional pseudostress, respectively.

The variances were also computed for the 2-year period at each buoy and for each component of pseudostress. The variances tended to be higher at the northern and western buoys, where there is strong directional variability. Averaging over all 34 buoys resulted in variances of 508 m^2/s^2 for the zonal pseudostress component and 399 m^2/s^2 for the meridional component.

IV. CONSTRUCTING MAPS BY OBJECTIVELY ESTIMATING THE PSEUDOSTRESS

Several sets of pseudostress fields were created from ECMWF winds, varying in temporal and spatial resolution, as listed in Table 2.

Table 2. Pseudostress fields used to develop mapping methodology.

Name of Pseudostress Field	Dates	Spatial Resolution	Temporal Resolution
FNMOC	3/93	1°	12 hours
ECMWF	1/9–3/93	1.125°	6 hours
ECMWF, spectrally modified ("true")	9/92–3/93	0.5°	1 day
ECMWF, spectrally modified, subsampled (synthetic NSCAT)	9/92–3/93	0.5°	1 day
ECMWF, spectrally modified, subsampled, mapped	9/92–3/93	2°	5 day

Daily pseudostress maps were made with two sets of winds: the spectrally modified ECMWF ("true") pseudostress values, which have been sampled in the NSCAT sampling pattern (synthetic NSCAT data), and the actual NSCAT wind data, which have been converted to pseudostress. Zonal and meridional components were mapped independently. Maps of the error estimates were also constructed. The map domain covers the tropical Pacific Ocean from 31°S to 31°N and from 124° to 74°E on a 1° × 1° grid. The maps are nominal 5-day averages with resolutions of 1° or 2°.

If scatterometer data were available on a regular temporal and spatial grid, similar to analysis wind products, then a simple boxcar filter could be used to obtain the temporal average. However, measurements are irregular in both time and space and on time scales that are short compared to the 41-day repeat cycle of ADEOS-I. Therefore, we use a method designed to produce a robust estimate of the temporal average when using data irregularly spaced in time (Chelton and Schlax, 1991). The problem of an irregular spatial grid is solved by binning all measurements within a given region for every 6-hour interval. Except in rare cases, described below, it was not necessary to spatially interpolate the data for the final map.

For a given spatial bin (grid point in the final map) many intervals will have no data, as shown in Figure 9. The Chelton/Schlax method is essentially a time integral of the traditional objective estimate (Bretherton et al., 1976) and produces an objective estimate of a temporal mean, as well as an error estimate for that mean. The weights applied to the measurements to

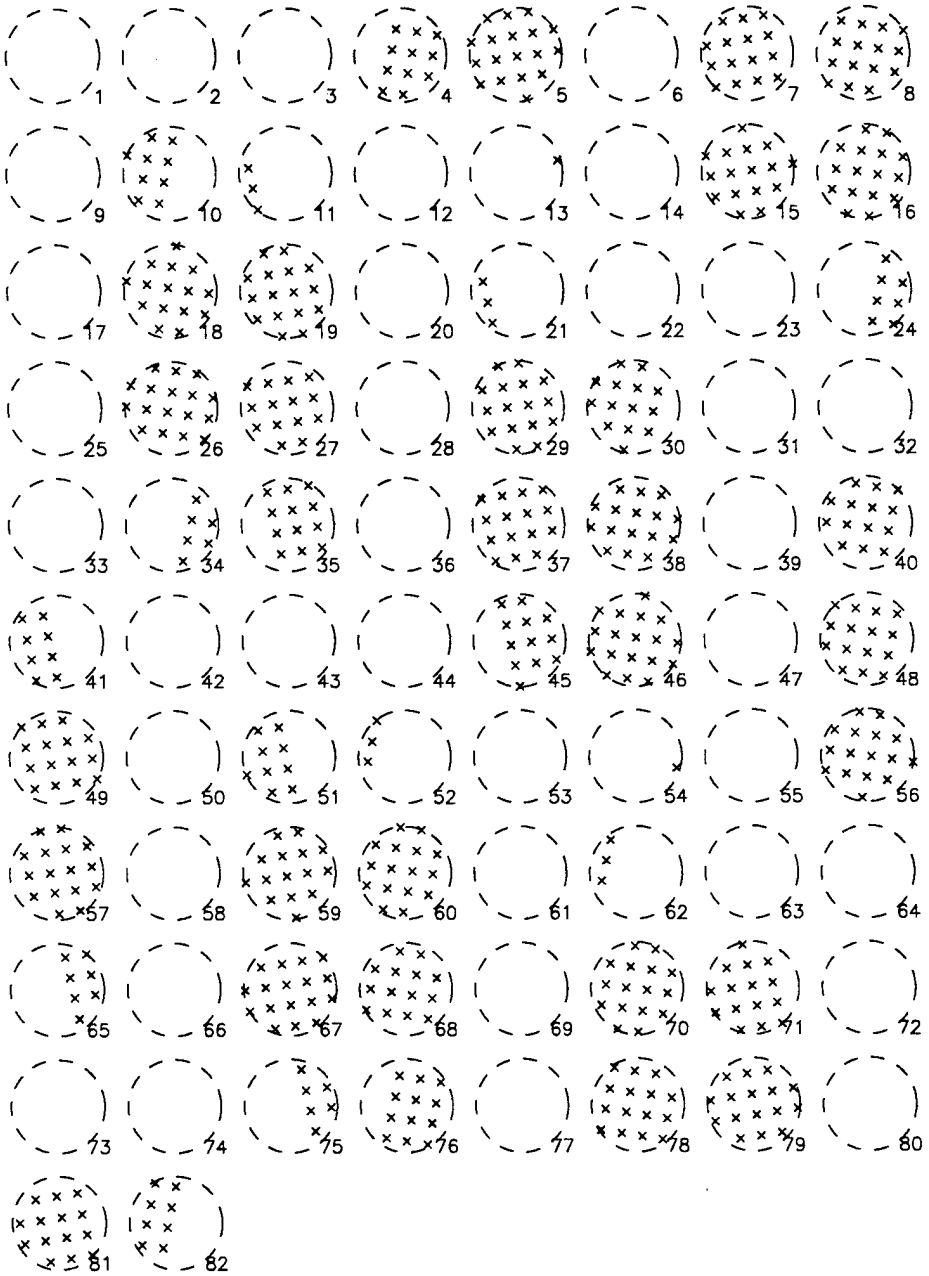

Figure 9. The number of NSCAT data points at 25-km resolution that fall within 1° radius of a grid point for the entire 41-day repeat cycle. Each succeeding circle is 12 hours later, showing the irregularity of the data in time.

obtain the mean are equivalent to a tapered boxcar filter, which is slightly wider than a boxcar filter, the weight depending on the temporal resolution desired.

Therefore, the map made for a particular day is a weighted average of data from that day plus data from the 2 days before and after it, totaling 5 days, plus some data before and after that interval, depending on the decorrelation time scale. The extended interval from which data were used included twice the *e*-folding scale of the signal covariance (49 hours for the zonal component and 29 hours for the meridional component). Figure 10 shows the temporal span of data used to compute a single 5-day mean pseudostress map (approximately 13 days for the zonal component).

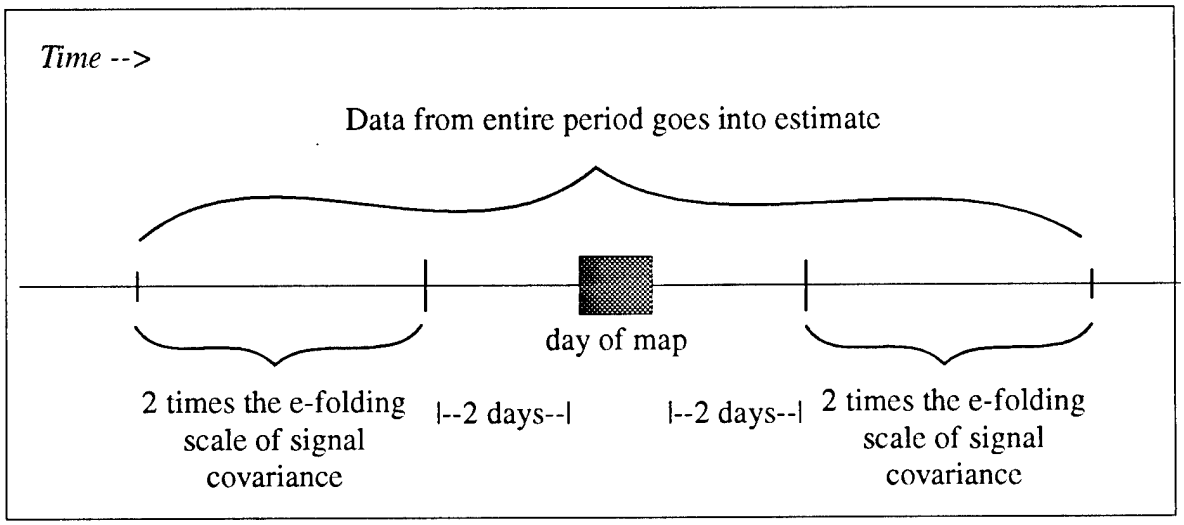

Figure 10. Temporal span of data for a nominal 5-day average.

All data within a 1° or 2° radius of a given grid point are extracted, binned, and averaged into 6-hour intervals to reduce the amount of data put into the optimal average. (This decreases the run time of the mapping procedure without loss of information.) For this average, the data are weighted as a function of distance to the grid point (Δr) using the weighting function $\exp(-\Delta r/L_s)$, where L_s is equal to 2°.

Before the objective estimate is made, the climatological mean pseudostress is removed. From the FSU monthly climatology, the first four harmonics are used to develop daily values at each grid point, similar to the values developed at the TAO buoy locations. These daily climatological FSU means are removed from the binned pseudostress values. After the objective estimate is made, the FSU mean is added back in. Figure 11 shows an example of the true mean (based on the complete modified ECMWF fields), a simple binned average, and the objective average.

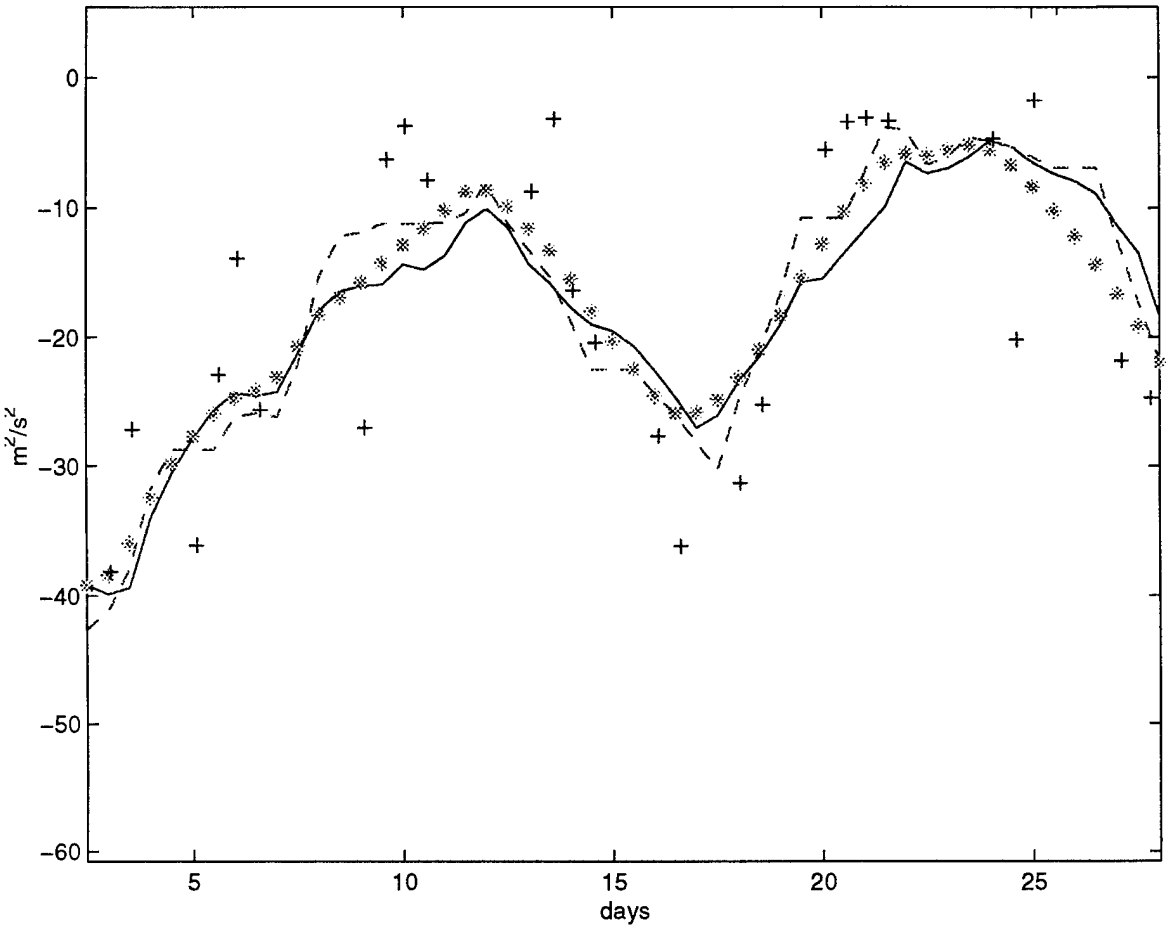

Figure 11. True (solid), binned (dashed), and objectively averaged (*) pseudostress, plotted against "synthetic" data (+) for a month of "true" winds.

Finally, the maps are checked for missing data and estimates that are more than three standard deviations from the local 3×3 grid-point mean. These values, which occur less than 1% of the time, are replaced with that local mean. An example of the zonal and meridional component pseudostress maps for the synthetic NSCAT data is shown in Figure 12 along with the "true" stress field components.

Maps of error estimates are also constructed. The error is derived from the objective estimate and is a function of the number of samples and their temporal lags relative to the map day, the covariances of the pseudostress, and the measurement error.

The objective estimate requires an estimate of the noise-to-signal ratio. Because individual measurements are first averaged, we compute the estimate based on an average pseudostress value as follows. The NSCAT specification for wind speed accuracy is 2 m/s or 10%, whichever is larger. Assuming 2 m/s and a typical speed of 6 m/s for the tropics gives a

wind speed error of about 33%. Assuming this also holds for each wind component, the conversion to stress doubles this value to 67%. Pseudostress values are first spatially averaged, which reduces instrument error, say by $N^{-1/2}$ where N depends on the spatial bin size and the spatial decorrelation of the instrument errors. A 2° bin contains about 10–14 actual measurements and, allowing for data correlations, gives perhaps four independent estimates, reducing pseudostress errors to 33%. The noise-to-signal ratio is based on variances and thus would be $(0.33)^2$, or 0.11. This ratio would be much larger for the 1° maps, where N would be only 1, or approximately 0.44.

V. ESTIMATED ERRORS: DETERMINING TEMPORAL AND SPATIAL RESOLUTION FOR THE MAPS

Appropriate experiments were performed in which the sizes of the temporal and spatial bins were varied to determine the map parameters. The spatial and temporal resolution was selected by examining the spatial structure of the estimated error field. Using altimeter data, Chelton and Schlax (1994) showed that map parameters that give relatively uniform error estimates produce fields with fewer spurious features from the instrument sampling pattern. The quantity used here to quantify the uniformity of the error field was the ratio of the (spatial) standard deviation of the errors to the (spatial) mean error. While the mean error always decreases as either the averaging interval or the spatial bin size is increased, the same is not true of this error ratio.

The top panel of Figure 13 shows the mean errors for various spatial bins and temporal averaging intervals. The bottom panel shows the error ratio. Our choice of 5 days and 2° (1° radius) should result in an error ratio of less than 10% and mean errors of about 5 m^2/s^2 for the pseudostress. Note that this error ratio is based on error standard deviation, rather than on maximum error as done by Chelton and Schlax (1994), and results in a somewhat less uniform error map. The error ratio for the 8 months of NSCAT maps is shown in Figure 14 for two conditions. The errors increase near land owing to a combination of more erroneous vectors and poorer coverage; the large errors near land result in an increase in the standard deviation of the errors. The error ratios computed *with* the error values near the coasts (within 50 km of land) range from about 20% down to about 14% (top row of dots in Figure 14). When the coastal error values are excluded, the error ratio hovers around 11%, only slightly higher than our target value. The presence of land and occasional data dropouts result in fewer than expected samples. However, our statistical studies were based on open ocean sampling with no data dropouts. Note also that around days 77 and 78 (15 and 16 January 1997) the error ratio is anomalously low. NSCAT was in high-resolution mode during that time; hence data are not available for those 2 days. The mean errors for those days and the few days before and after are therefore anomalously high.

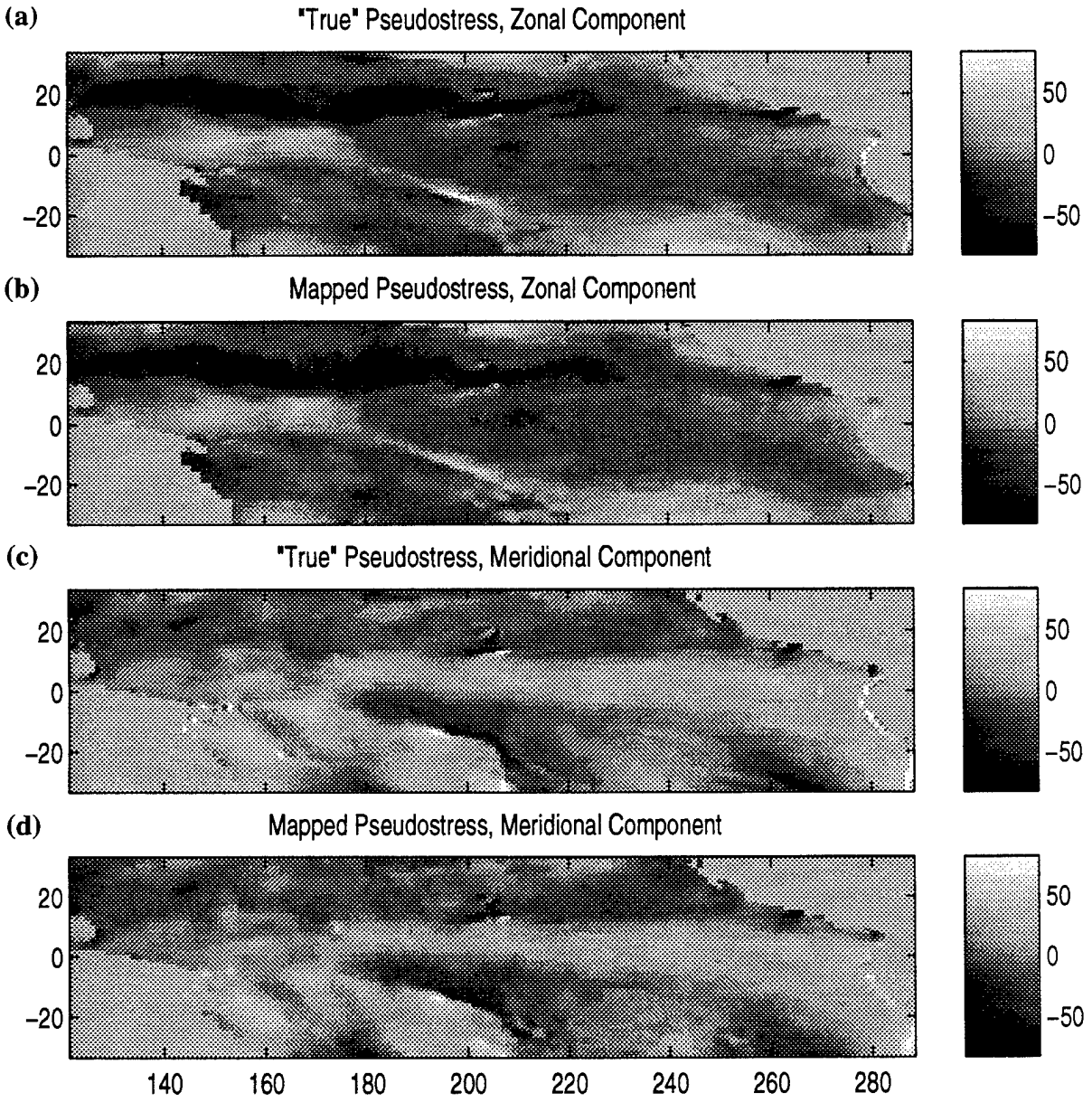

Figure 12. (a) and (c) are the zonal and meridional "true" pseudostress fields, respectively, and (b) and (d) are the zonal and meridional mapped pseudostress fields for 15 November 1992, all in meters^2/seconds^2.

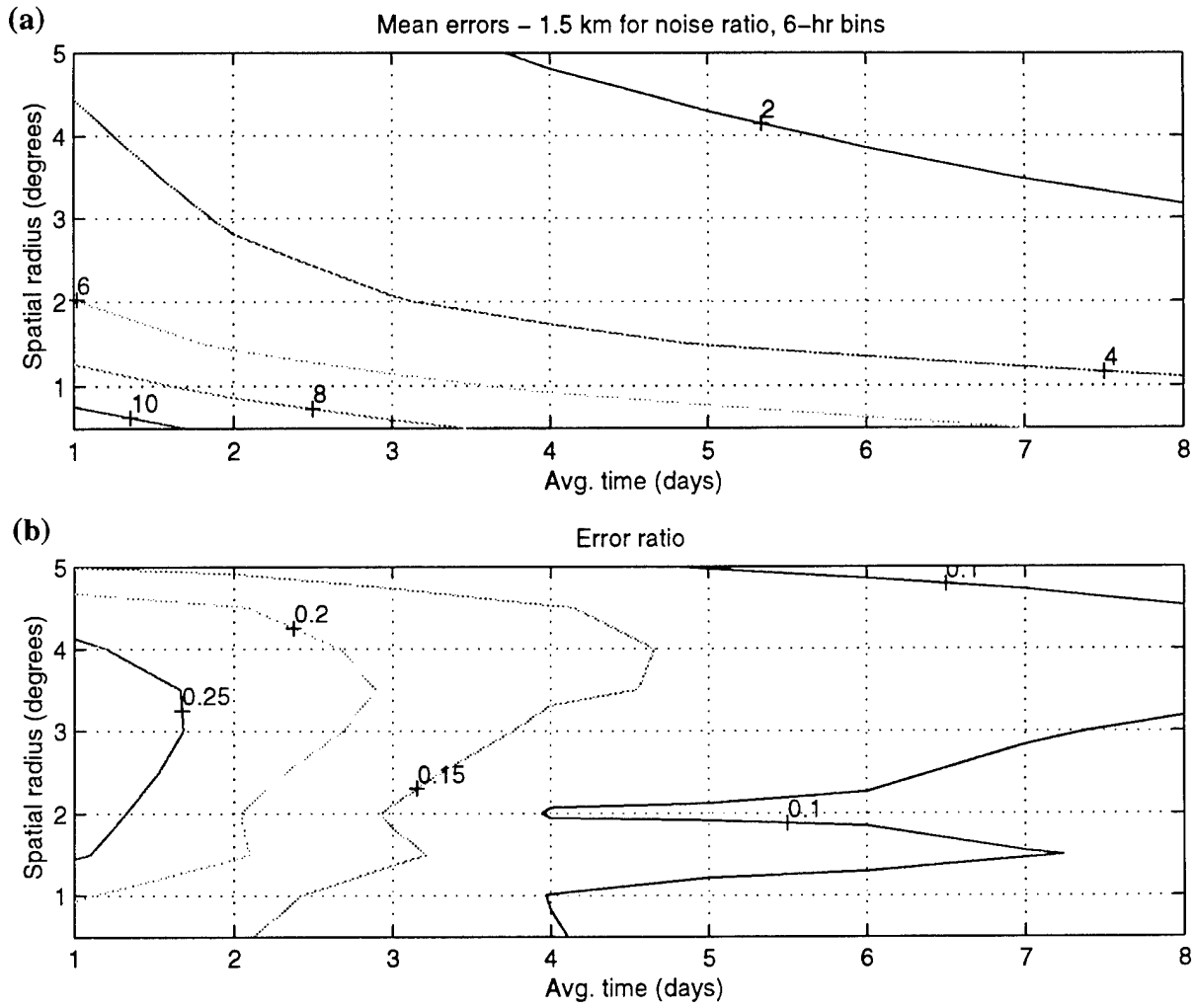

Figure 13. (a) Mean errors as a function of varying spatial and temporal bin sizes. (b) Error ratio for these spatial and temporal bins. The error ratio is defined as the spatial standard deviation of the error divided by the spatial mean error.

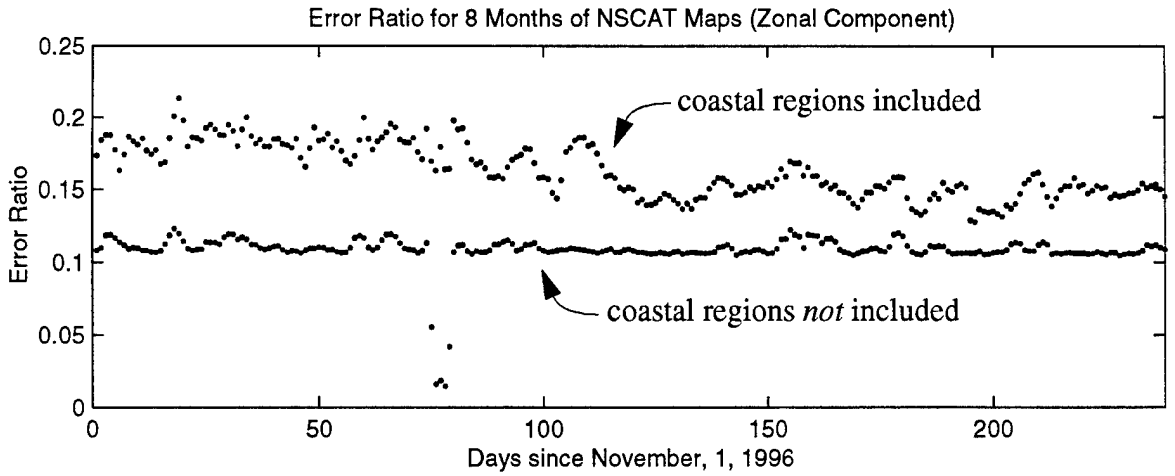

Figure 14. Error ratio, as defined in the text, for the error estimates (from the objective mapping algorithm) for the 8 months of the zonal component of pseudostress from NSCAT maps. The top row of dots shows the error ratio with the coastal regions included, and the bottom row shows the error ratio with those areas removed.

The normalized estimated errors for the NSCAT maps and the maps made with synthetic NSCAT data don't vary much over the map domain, by design. (The errors are normalized by dividing by the square root of the signal variance.) For the study of estimated errors, a constant variance was used: 500 and 400 $(m^2/s^2)^2$ for the zonal and meridional pseudostress variance, respectively, as discussed at the end of Section 3. Figure 15 shows the time-averaged normalized estimated errors for the entire basin and as a function of latitude. They are very uniform, as expected, except in the region near Baja California, where substantially less data were available owing to calibration tests of the scatterometer performed over the western U.S.

The actual errors (mapped pseudostress minus "true" pseudostress) increase with latitude, as shown by the circles in Figure 16, owing to the increase of variance with latitude, as shown by the solid lines in the same figure. The estimated errors as a function of latitude are shown by the stars. The actual errors and the estimated errors are very similar in magnitude and in their broad dependence on latitude. These results confirm that the algorithm is working properly. The scallop pattern of the errors is a result of averaging the argyle pattern of errors shown in Figure 15. The values of both the estimated errors and the normalized estimated errors for the NSCAT data maps are similar to those of the synthetic maps.

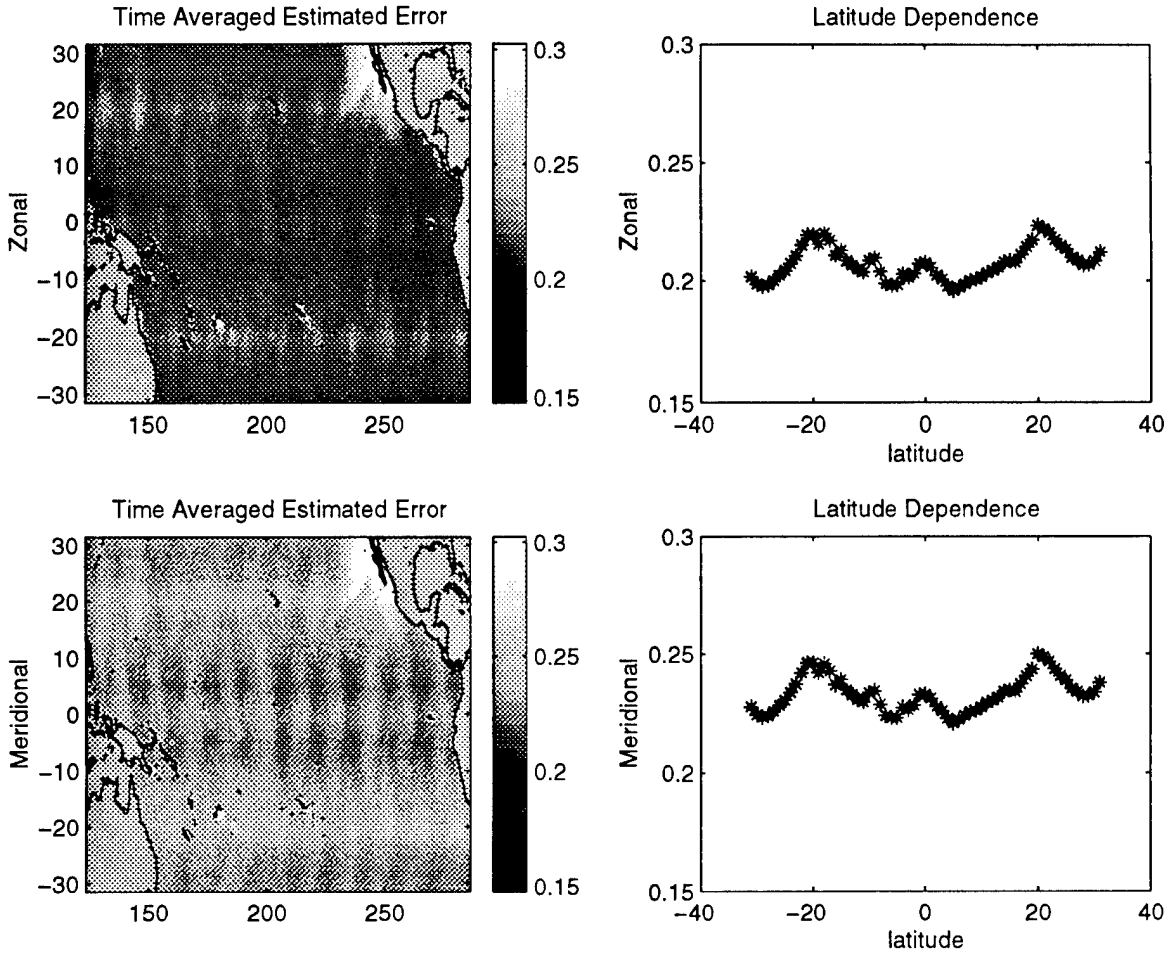

Figure 15. Normalized estimated errors, time averaged over the 8-month data set of NSCAT. Left panels show errors over the basin (normalized by the signal variance) for zonal and meridional pseudostress, respectively. Right panels show these errors (zonally averaged) as a function of latitude.

Spectral analysis of the NSCAT pseudostress maps was performed to determine if the sampling pattern can be found in the maps. The inner portion of the maps, from 23°S to 23°N and from 151°E to 211°W, which contains no large land masses, was used for this analysis. The zonal and meridional spectra of the zonal component of the pseudostress are plotted in Figure 17 on the left and right sides, respectively, along with the $k^{-1.8}$ spectrum (solid line) for reference. The top panels show the spectra for the 1° and 2° mapped NSCAT pseudostresses and for the ECMWF 5-day tapered means. The bottom panels show the spectra for the "true" pseudostress as well as for the 1° and 2° synthetic (mapped) pseudostresses. Freilich and Chelton (1986) estimated the spectral slope of both the winds and the energy (square of the winds) to be approximately $k^{-1.8}$. As discussed in Section 2, the energy in the ECMWF winds falls off for the higher frequencies. The 1° and 2° NSCAT maps contain higher energy all the way out to the Nyquist wavenumber (which is two times the grid spacing), with the 1° maps

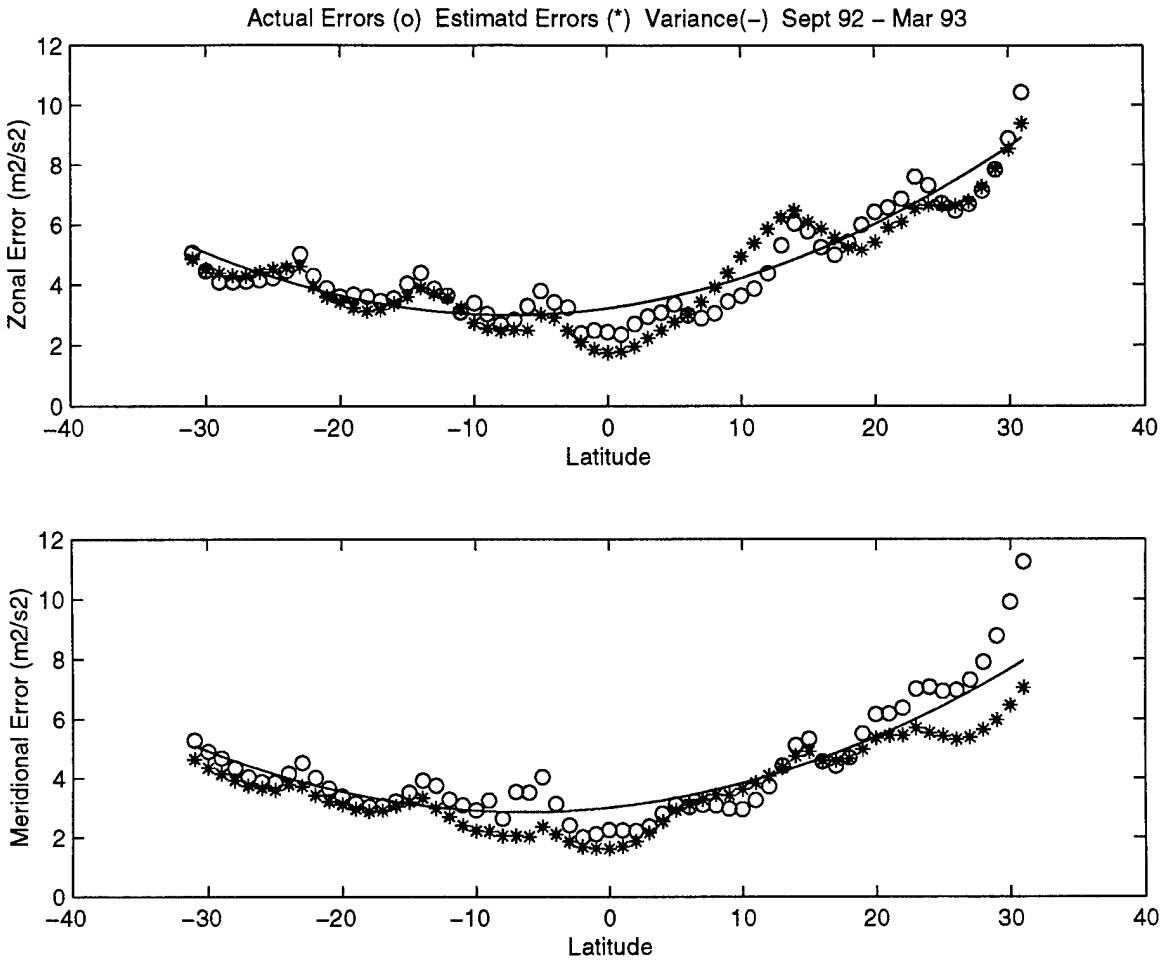

Figure 16. Actual errors (mapped pseudostress minus "true") as a function of latitude, shown by open circles, for zonal (top panel) and meridional (bottom panel) pseudostress, in meters^2/second^2. Estimated errors as a function of latitude are shown by the stars. The solid lines represent the standard deviation of the pseudostress as a function of latitude, reduced by a factor of 5 (zonal) and 4 (meridional), to show that the errors and the variance have the same dependence on latitude.

containing the highest energy levels as might be expected. This confirms that the maps do have the resolution of 1° and 2°, respectively. However, in both the 1° and 2° zonal spectra in the left panels, there is a bump near the swath width of 600 km. The bar on the abscissa shows the location of 1/600 km. We attribute this bump in energy in part to sampling-pattern artifacts in the maps. This energy bump is also evident in the zonal spectra of the synthetic pseudostress but not in any of the meridional spectra, confirming that it is an artifact of the mapping process. So although there is indeed 2° resolution in the 2° maps, there is also some energy from the sampling pattern of the NSCAT.

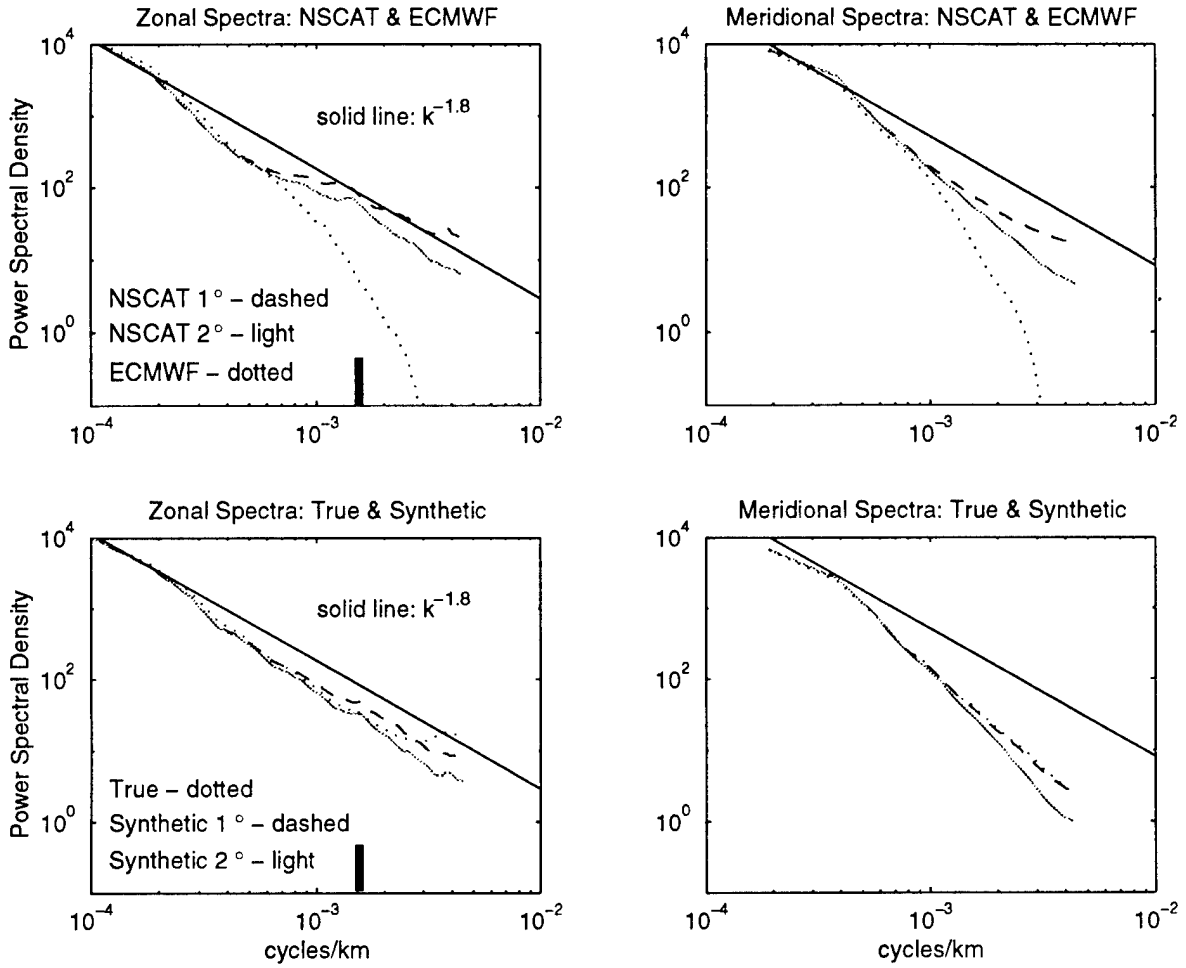

Figure 17. Power spectral density of the zonal component of pseudostress for the NSCAT and ECMWF data sets (top panels) and for the "true" and synthetic data sets (lower panels). Left and right panels show the zonal and meridional spectra, respectively. The solid straight line represents the $k^{-1.8}$ spectrum. The black bars on the abscissas of the left panels represent the 1/600-km cutoff of the ECMWF analyses as well as the swath width of the NSCAT.

VI. MODEL TESTING OF MAPPING METHODOLOGY

Several sets of pseudostress fields created from ECMWF winds, listed in Table 2, were used to force an ocean circulation model. The data sets include the original ECMWF pseudostress fields, spectrally modified ECMWF or "true" fields, synthetic NSCAT data mapped into daily fields, and the actual NSCAT data mapped into daily pseudostress fields. Studying the sensitivity to map resolution and errors determines the most appropriate parameters of the maps for ocean circulation study. However, this is the subject of another study.

VII. NSCAT DATA MAPS

The NSCAT data are estimates of the wind at 10 m above the ocean, which are converted to pseudostress before mapping. The data set begins in September, but continuous data are not available until late October. Our daily, 5-day running average maps begin 1 November 1996 and run through 26 June 1997. An example of real NSCAT data mapped with our mapping algorithm is shown in Figure 18, which also includes the component differences between the mapped NSCAT data and a 5-day tapered mean of the ECMWF 10-m analysis winds (also converted to pseudostress). In general, the NSCAT data measure a stronger Intertropical Convergence Zone than is present in the analyses.

There is one issue with the NSCAT data that is as yet unresolvable. There are occasional 180° ambiguities in the direction of the wind. These flipped vectors are discussed in some detail in a technical report being written at the Woods Hole Oceanographic Institution, Evaluation of NSCAT Scatterometer Winds Using Equatorial Pacific Buoy Observations. According to comparisons with TAO data, the flipped vector occurs about 4–5% of the time (personal communication, Michael Caruso). However, we have no way of flagging these flipped vectors and therefore cannot correct them or even statistically characterize them to determine their impact on our maps or their contribution to the errors.

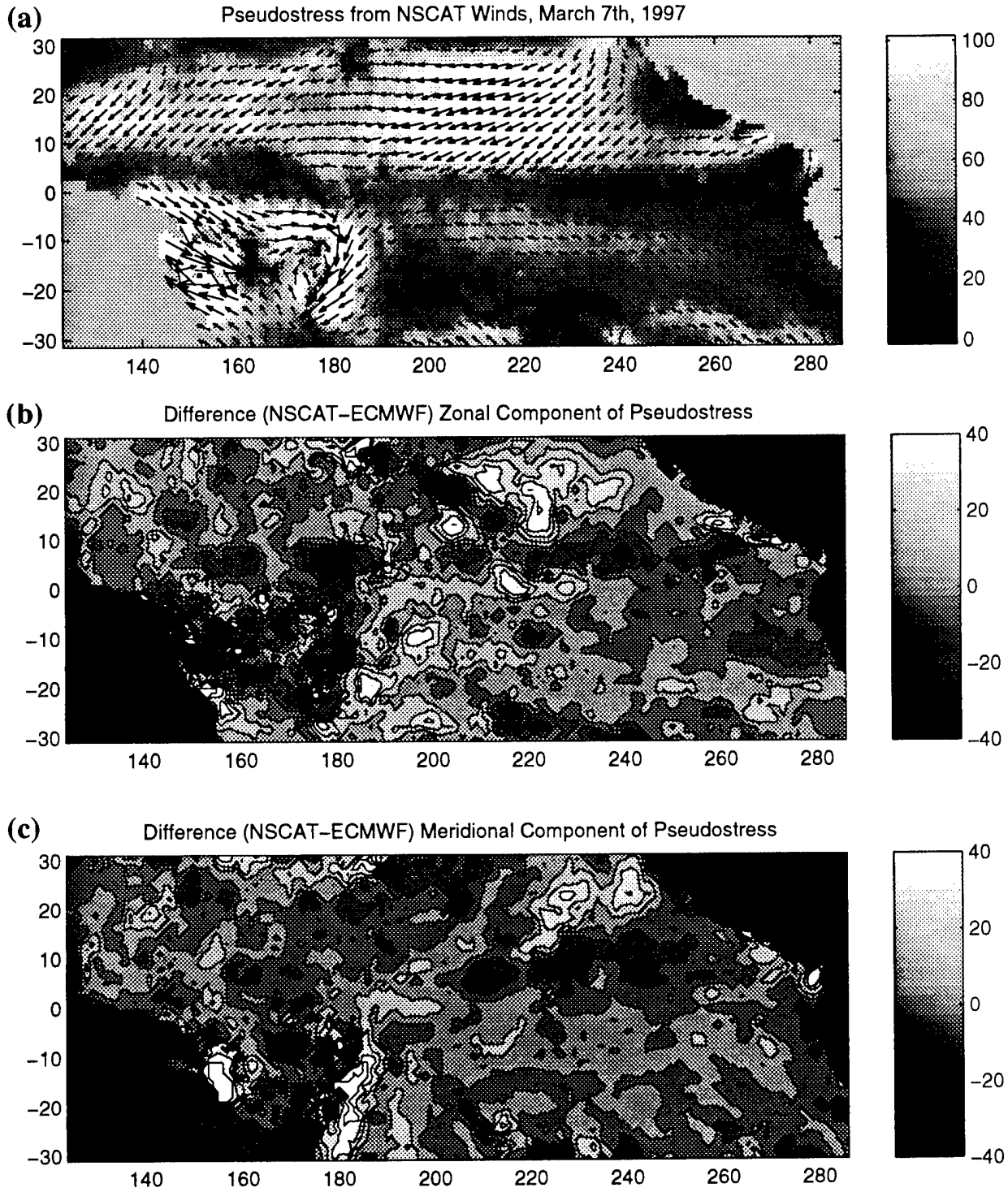

Figure 18. (a) Example of pseudostress (m^2/s^2) mapped from NSCAT data for 7 March 1997 showing a strong westerly wind burst in the western Pacific Ocean. Differences in pseudostress (NSCAT minus ECMWF) for (b) zonal component and (c) meridional component for the same day.

REFERENCES

Bretherton, F.P., R.E. Davis, and C.B. Fandry, 1976. A technique for objective analysis and design of oceanographic experiments applied to MODE-73, *Deep-Sea Res.*, **23**, 559–582.

Chelton, D.B., and M.G. Schlax, 1994. The resolution capability of an irregularly sampled dataset with application to Geosat altimeter data, *J. Atmos. Ocean Technol.*, **11**, 534–550.

Chelton, D.B., and M.G. Schlax, 1991. Estimation of time-averaged chlorophyll concentration from irregularly spaced satellite observations, *J. Geophys. Res.*, **96**, 14,669–14,692.

Freilich, M.H., and D.B. Chelton, 1986. Wavenumber spectra of Pacific winds measured by the Seasat Scatterometer, *J. Phys. Oceanogr.*, **16**, 741–757.

Kelly, K.A., and M.J. Caruso, 1990. A modified objective mapping technique for scatterometer wind data, *J. Geophys. Res.*, **95**, 13,483–13,496.

McPhaden, M.J., 1995. The Tropical Atmosphere Ocean Array is completed, *Bull. Am. Met. Soc.*, **76**, 739–741.

REPORT DOCUMENTATION PAGE

Form Approved
OPM No. 0704-0188

1. AGENCY USE ONLY *(Leave blank)*	2. REPORT DATE	3. REPORT TYPE AND DATES COVERED
	April 1998	Technical

4. TITLE AND SUBTITLE
Establishing A Mapping Methodology For NSCAT Winds

5. FUNDING NUMBERS
NASA Contract 960927
UW-NOAA Cooperative Agreement NA67RJ0155

6. AUTHOR(S)
S. Dickinson, S. Singh, K.A. Kelly, M. Spillane, and M.J. McPhaden

7. PERFORMING ORGANIZATION NAME(S) AND ADDRESS(ES)
Applied Physics Laboratory
University of Washington
1013 NE 40th Street
Seattle, WA 98105-6698

8. PERFORMING ORGANIZATION REPORT NUMBER
APL-UW TR 9801

9. SPONSORING / MONITORING AGENCY NAME(S) AND ADDRESS(ES)

Tim Liu	Lee Dantzler	Eric Lindstrom
Jet Propulsion Lab, MS 300-323	NOAA/NESDIS, Code E	Phys. Ocean. Program
California Institute of Tech.	4700 Silver Hill Rd., MS 9909	NASA Headquarters
4800 Oak Grove Drive	Washington, DC 20233-9909	Washington, DC 20546
Pasadena, CA 91109		

10. SPONSORING / MONITORING AGENCY REPORT NUMBER

11. SUPPLEMENTARY NOTES

12a. DISTRIBUTION / AVAILABILITY STATEMENT
Approved for public release; distribution is unlimited.

12b. DISTRIBUTION CODE

13. ABSTRACT *(Maximum 200 words)*

A methodology is presented for mapping swath-oriented NASA scatterometer (NSCAT) wind data into gridded maps suitable for forcing ocean circulation models. NSCAT samples the winds over the equatorial Pacific Ocean unevenly in both space and time, and care must be taken in mapping them onto a grid to prevent aliasing the fields. It was necessary to develop a "true" wind field with which to test the mapping methodology. Prior to the availability of NSCAT data, the European Centre for Medium-Range Weather Forecasts (ECMWF) and Fleet Numerical Meteorology and Oceanography Center (FNMOC) analysis wind fields were studied. Spectral analysis of the ECMWF and FNMOC wind fields showed a drastic drop in energy at scales smaller than 600 km. These energy levels were "pumped up" in the Fourier domain to represent a true wind field more accurately. These "true" wind fields were converted to pseudostress, subsampled with the known NSCAT sampling pattern (termed "synthetic NSCAT" winds), and then objectively averaged. A study of the expected errors of the mapped pseudostress was conducted using a covariance function of the equatorial Pacific wind field determined with data from the Tropical Atmosphere Ocean (TAO) buoy array. A 5-day, 2° resolution was chosen for the daily mapped pseudostress. Comparisons of the "true" winds converted to pseudostress and the mapped synthetic NSCAT pseudostress show errors consistent with the expected values. Maps made of actual NSCAT data are also presented and discussed.

14. SUBJECT TERMS
Scatterometer, mapping winds, ocean, NSCAT, Pacific, tropical

15. NUMBER OF PAGES
28

16. PRICE CODE

17. SECURITY CLASSIFICATION OF REPORT	18. SECURITY CLASSIFICATION OF THIS PAGE	19. SECURITY CLASSIFICATION OF ABSTRACT	20. LIMITATION OF ABSTRACT
Unclassified	Unclassified	Unclassified	SAR